Communications in Physics, Vol. 36, No. 1 (2026), pp. 81-90
DOI: https://doi.org/10.15625/0868-3166/23622

Highly photoluminescent blue–green carbon quantum dots synthesized via plasma solution interaction for bioimaging applications

P. V. Duong[1], **Nguyen Minh Hoa**[2], **Do Minh Hieu**[1], **Vu Van Thu**[3], **Nguyen Dac Dien**[3], **Le Duc Toan**[4], **Le Anh Thi**[5,6,†], **S. A. Tikhomirov**[7] **and Nguyen Thanh Binh**[1,‡]

[1]*Institute of Physics, Vietnam Academy of Science and Technology, 10 Dao Tan, Giang Vo, Hanoi 10000, Vietnam*

[2]*Faculty of Fundamental Sciences, Hue University of Medicine and Pharmacy, Hue University, Hue, Vietnam*

[3]*Faculty of Occupational Safety and Health, Vietnam Trade Union University, Hanoi 10000, Vietnam*

[4]*Natural Sciences Department, Phu Yen University, Tuy Hoa City, Phu Yen, Vietnam*

[5]*Institute of Research and Development, Duy Tan University, Da Nang 550000, Vietnam*

[6]*Faculty of Natural Sciences, Duy Tan University, Da Nang 550000, Vietnam*

[7]*B. I. Stepanov Institute of Physics of the National Academy of Science of Belarus, Minsk, Belarus*

E-mail: [†]leanhthi@duytan.edu.vn; [‡]tbnguyen@iop.vast.vn

Received 14 October 2025
Accepted for publication 11 December 2025
Published 5 March 2026

Abstract. *Blue (B-CQDs) and green (G-CQDs) carbon quantum dots with exceptional photoluminescence were synthesized using a plasma solution interaction (PSI) method, employing glucose as an environmentally friendly carbon source. The PSI process enabled rapid, catalyst-free synthesis with tunable optical properties by varying plasma exposure time. Both types of carbon quantum dots consist of uniformly dispersed spherical nanoparticles (3–5 nm), with partially graphitic cores and a lattice spacing of 0.21 nm corresponding to the (100) plane of graphite. The B-CQDs emit intense blue light at 450 nm, with a quantum yield of 21%, while the G-CQDs display strong green emission at 515 nm, yielding a quantum yield of 19%. Structural and spectroscopic analyses indicate that blue emission results from intrinsic π–π^* transitions within sp^2-hybridized carbon domains, whereas green emission originates from surface or defect-state n–π^* transitions linked to oxygen-containing groups formed during prolonged plasma treatment. Both types of CQDs*

exhibit excellent aqueous stability, photostability, and biocompatibility, with strong intracellular fluorescence observed in preliminary bioimaging tests. These findings underscore plasma solution interaction as an efficient, controllable method for producing color-tunable CQDs with potential for optical and biological applications.

Keywords: carbon quantum dots; plasma solution interaction; glucose precursor; photoluminescence; quantum yield; bioimaging.

Classification numbers: 81.05.U-; 81.05.uj; 68.35.bm; 52.77.Bn; 73.20.Mf; 52.40.-w.

1. Introduction

Carbon Quantum Dots (CQDs) are a class of zero-dimensional carbon-based nanomaterials known for their tunable photoluminescence, high photostability, low toxicity, and excellent aqueous dispersibility [1, 2]. These properties make CQDs ideal candidates for applications in fluorescence imaging, biosensing, catalysis, light-emitting diodes (LEDs), and energy-conversion devices [3–6]. Since their discovery in 2004, CQDs have been seen as promising alternatives to semiconductor quantum dots, offering low-cost synthesis, biocompatibility, and environmental stability [7]. The fluorescent behavior of CQDs is highly dependent on their size, structure, surface chemistry, and synthesis conditions. The emission mechanisms are generally classified into two types: (i) intrinsic π–π^* transitions within sp^2-hybridized graphitic domains (blue emission) and (ii) surface or defect-related n–π^* transitions from oxygen-, nitrogen-, or sulfur-containing groups (green to red emission) [8, 9]. Achieving control over these emissions is crucial for designing high-efficiency, color-tunable CQDs.

Traditional synthesis methods, such as hydrothermal and solvothermal processes, often require high temperatures, long reaction times, and the use of harsh chemicals [1]. In contrast, plasma-based methods like plasma solution interaction offer a rapid, eco-friendly, and catalyst-free route for synthesizing CQDs [9–12]. Plasma solution interaction works at room temperature, using plasma to induce carbonization and surface passivation in a single step, allowing fine control over the optical properties by adjusting plasma exposure time. Despite the growing interest in plasma solution interaction for CQD synthesis, the effects of plasma exposure on emission properties, quantum yield, and the transition between core- and surface-dominated emissions are not fully understood. This study aims to fill this gap by synthesizing blue-emitting (B-CQDs) and green-emitting (G-CQDs) CQDs using glucose as the carbon source. By varying plasma exposure time, we can tune the emission color from blue (450 nm) to green (515 nm). The shorter plasma treatment results in partially graphitic CQDs with blue emissions, while prolonged exposure increases surface oxidation, leading to green emissions.

The resulting CQDs exhibit high quantum yields (21% for B-CQDs and 19% for G-CQDs), excellent photostability, and strong fluorescence even under continuous UV exposure. Additionally, the CQDs show good aqueous stability and low cytotoxicity, making them ideal for bioimaging applications. Preliminary tests confirm that both B-CQDs and G-CQDs penetrate cellular membranes and provide bright, stable fluorescence in cells. This study demonstrates plasma solution interaction as an efficient, environmentally friendly method for synthesizing color-tunable, biocompatible CQDs, offering valuable insights into the relationship between plasma exposure, surface chemistry, and photoluminescence mechanisms. The findings highlight the potential of plasma solution interaction derived CQDs for a wide range of optical and biological applications.

2. Experiment

2.1. Materials

Analytical grade D(+)-glucose ($C_2H_{12}O_6$, $\geq$ 99.5%) was purchased from Sigma-Aldrich and used without further purification. Ultrapure deionized (DI) water (18.2 MΩ cm resistivity) was used in all preparations. No organic solvents, surfactants, or stabilizing agents were introduced to maintain the green chemistry nature of the process.

2.2. Synthesis of blue and green carbon dots

B-CQDs and G-CQDs were synthesized via plasma solution interaction using glucose as the carbon precursor. A dielectric barrier discharge plasma, connected to a 15 kV, 20 kHz AC power supply, generated the plasma plume in ambient air. This plume was directed onto a 0.1 M glucose solution in a quartz reactor (50 mL), with the plasma nozzle positioned 10 mm from the liquid surface. Plasma exposure initiated glucose decomposition and carbonization, with exposure times crucial for tuning the emission color: B-CQDs exposed for 15 minutes, resulting in partial carbonization and graphitic core formation. While G-CQDs exposed for 30 minutes, leading to increased oxidation and surface defects. The initial colorless solution turned pale brown, indicating carbonization. After exposure, the suspensions were centrifuged, filtered, and stored at 4°C. Both B-CQDs and G-CQDs dispersions remained stable for several months without precipitation.

2.3. Characterization

The optical and structural properties of the synthesized carbon dots were characterized using a combination of spectroscopic and microscopic techniques. UV–Visible absorption spectroscopy recorded on a Shimadzu UV-2600 spectrophotometer. Photoluminescence (PL), excitation spectra, Time-resolved photoluminescence (TRPL) and Quantum yield (QY) measured on an Edinburgh Instruments FLS1000 spectrofluorometer. Fourier-transform infrared (FTIR) spectroscopy performed on a Bruker Tensor 27 spectrometer. Transmission electron microscopy (TEM) images were obtained with a JEOL JEM-2100 microscope operating at 200 kV.

2.4. Bioimaging evaluation

Biocompatibility and imaging potential of B-CQDs were assessed using HeLa cells. The cells were incubated with B-CQDs (100 µg/mL) for 4 hours at 37°C under 5% CO_2, then washed with PBS to remove unbound dots. Imaging was performed using a confocal microscope (Leica TCS SP8) with excitation at 360 nm and emission recorded in the 420–600 nm range. Cell morphology and fluorescence intensity were analyzed to evaluate cytocompatibility and imaging performance.

3. Results and discussion

3.1. Morphology and structure

The morphology, size, and dispersion of the synthesized CQDs were characterized using TEM. The B-CQDs (Fig. 1a) exhibit a uniform quasi-spherical shape with no observable aggregation, suggesting excellent dispersibility. The size distribution histogram (inset) derived from over 100 individual measurements reveals a narrow distribution with a mean particle diameter of 4.2 nm, as determined by Gaussian fitting. Similarly, the G-CQDs (Fig. 1b) show uniform spherical

morphology with good dispersion on the carbon grid. The statistical analysis of the size distribution (inset) shows that the average diameter of the G-CQDs is slightly smaller at 3.8 nm. These results confirm the successful synthesis of monodispersed carbon quantum dots in both B-CQDs and G-CQDs, with only a minor size difference. The slight variation in size between the two types of CQDs is unlikely to significantly impact their optical properties, suggesting that the observed differences in emission behavior are primarily due to surface chemistry and electronic structure rather than quantum confinement effects.

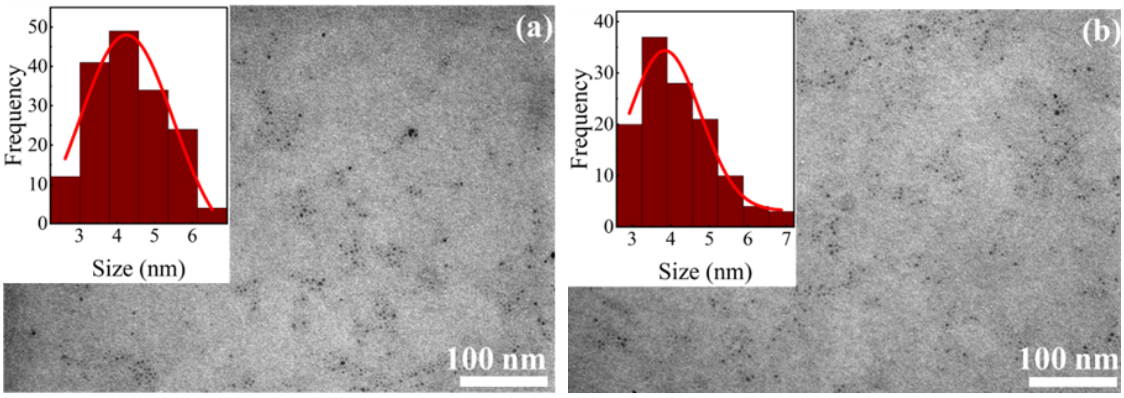

Fig. 1. TEM images of (a) B-CQDs, (b) G-CQDs (Insets are the size distribution histograms of CQDs).

3.2. Surface functional groups

The surface functional groups of the B-CQDs and G-CQDs were analyzed using FTIR spectroscopy. As shown in Fig. 2, both samples exhibit characteristic absorption bands indicative of abundant oxygen-containing groups, but with notable differences in their relative intensities. A strong, broad absorption band centered at approximately 3400 cm^{-1} dominates the spectra of both sample, corresponding to the O-H stretching vibrations from hydroxyl and carboxyl groups, as well as adsorbed water molecules [13, 14]. This suggests that both types of CQDs possess highly hydrophilic surfaces. At lower wavenumbers, a distinct peak near 1700 cm^{-1} appears, which is attributed to the C=O stretching vibration of carboxyl (-COOH) or carbonyl groups [3]. Another prominent peak around 1620 cm^{-1} is associated with the C=C stretching of the sp^2-hybridized carbon core and potentially the bending vibrations of N-H groups. The presence of C-O bonds is confirmed by several peaks in the 1000-1400 cm^{-1} range, characteristic of ether, epoxy, and hydroxyl functionalities [3]. A comparative analysis reveals significant differences in the surface chemistry

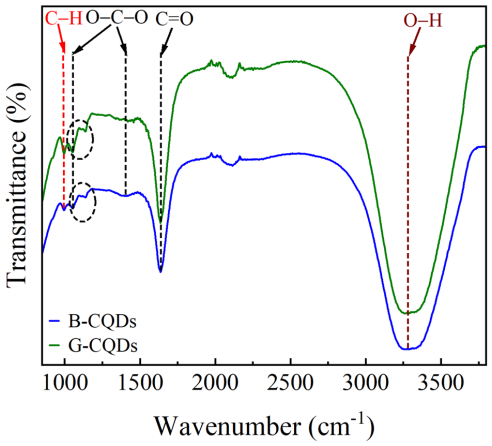

Fig. 2. (Color online) FTIR spectra of B-CQDs (blue line) and G-CQDs (green line).

of the two samples. The B-CQDs (blue line) show a more intense and broader O-H band and a sharper C=O absorption peak compared to the G-CQDs. This indicates that B-CQDs have a higher density of hydroxyl and carboxyl groups on their surfaces. Conversely, the G-CQDs (green line) exhibit well-resolved peaks in the C-O stretching region (1000-1200 cm^{-1}), suggesting a greater prevalence of ether or epoxy groups compared to carboxyl functionalities. The FTIR analysis confirms that both B-CQDs and G-CQDs are functionalized with a variety of oxygen-containing groups, with the B-CQDs exhibiting a higher degree of surface oxidation. This difference in surface chemistry is likely to contribute to the observed variations in photoluminescence behavior and excited-state dynamics between the two types of quantum dots.

3.3. Optical properties

The optical properties of the B-CQDs and G-CQDs were systematically investigated using UV-Vis absorption, PLE, and PL spectroscopy. These analyses provide insights into the electronic structure, emission behavior, and potential application suitability of both types of quantum dots. As shown in Figs. 3a and 3b, both samples display two main absorption bands located near 300 nm and 400 nm, which correspond to the π–π^* transition of the sp^2-hybridized carbon core and the n–π^* transition of oxygen-containing surface groups, respectively [15]. These transitions arise from the interplay between the conjugated carbon core and the surface functional groups that modulate electronic states. Although the overall absorption profiles of B-CQDs and G-CQDs are similar, the differences in their emission behavior originate from the distinct balance between core and surface electronic states induced by different plasma exposure times.

The PLE spectra of B-CQDs and G-CQDs (Figs. 3a and 3b) were measured to explore the excitation-dependent emission behavior. Both types of quantum dots exhibit a broad excitation range, peaking at approximately 400 nm, which aligns with the absorption features observed in the UV-Vis spectra. This excitation peak corresponds to the n–π^* transition and reflects the effective excitation of surface states, which dominate the emission characteristics of these dots. The PLE spectra for both types of quantum dots also show a gradual tail extending into the ultraviolet region, indicating that both surface-related and core-related transitions contribute to the overall photophysical behavior. This broad excitation range is an important feature for practical applications in optoelectronics and bioimaging, as it allows these quantum dots to be efficiently excited by widely available light sources, such as UV LEDs or lasers. The high excitation efficiency of both B-CQDs and G-CQDs suggests that the surface functionalities which control electron trapping and recombination pathways play a significant role in their photoluminescent properties.

The PL spectra of B-CQDs and G-CQDs (Figs. 3a and 3b) reveal distinct emission peaks that are strongly dependent on the excitation wavelength. The B-CQDs exhibit an intense blue emission centered at 450 nm when excited at 405 nm, which corresponds to the π–π^* transition within the carbon core. This blue emission indicates the presence of highly conjugated graphitic domains in the core, which are responsible for the shorter-wavelength emission. On the other hand, the G-CQDs display a prominent green emission centered at 515 nm under 405 nm excitation, which is attributed to n–π^* transitions from surface states and oxygen-containing functional groups. The green emission observed in G-CQDs is red-shifted compared to the blue emission of B-CQDs, which can be attributed to the increased surface oxidation and the formation of additional surface trap states that slow down the electron recombination process, resulting in the longer-wavelength green emission. In both cases, the PL intensity of G-CQDs is slightly higher

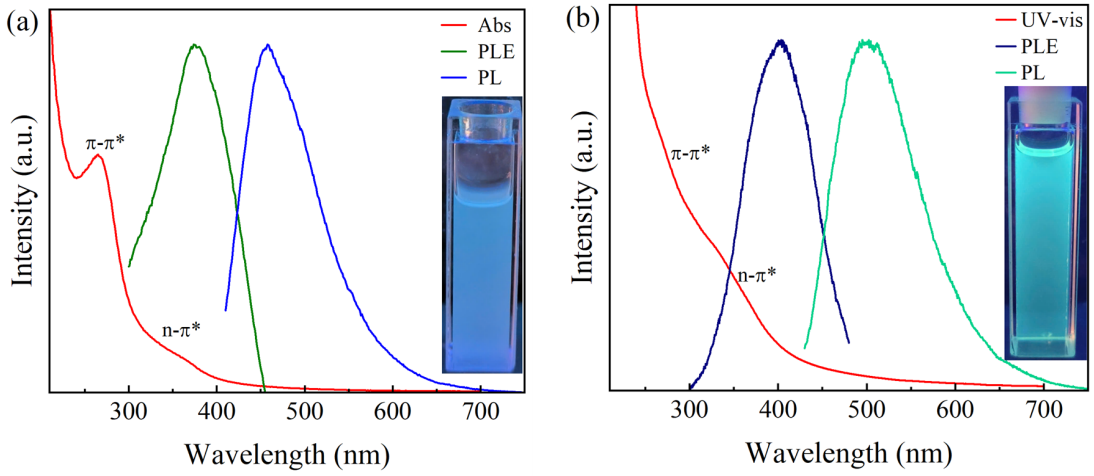

Fig. 3. (Color online) UV-vis absorption, Normalized PLE, and PL spectra (λ_{ex} = 405 nm) of (a) B-CQDs, (b) G-CQDs.

than that of B-CQDs, suggesting that G-CQDs have more efficient radiative recombination compared to their blue-emitting counterparts. This could be due to the more favorable interaction between the surface oxygenated groups and the carbon core, leading to enhanced PL efficiency in the green region [8]. Furthermore, the overall emission width for both B-CQDs and G-CQDs is relatively broad, which is indicative of the heterogeneous nature of the electronic states in both the carbon core and surface functional groups.

The distinct emission profiles of B-CQDs and G-CQDs clearly illustrate the competitive roles of core and surface states in defining their photoluminescence. The blue emission from B-CQDs is primarily attributed to intrinsic π–π^* transitions from the conjugated sp^2 carbon core, while the green emission from G-CQDs arises from surface-related n–π^* transitions due to oxygen- and nitrogen-containing groups. The higher PL quantum yield of G-CQDs (21%) compared to B-CQDs (19%) further supports the hypothesis that the surface passivation and functionalization in G-CQDs result in a more efficient radiative recombination process. In both cases, the excitation-dependent emission behavior of the CDs suggests the presence of multiple emissive states within both the core and surface, likely due to the heterogeneity in the size, shape, and functionalization of the quantum dots. These tunable emission properties make both types of quantum dots highly versatile for use in bioimaging, optoelectronic devices, and sensing applications, where specific color emissions are required.

Compared with previous studies using plasma solution interaction for CQD synthesis [**?**], the CQDs produced in this work exhibit several notable improvements. The quantum yields of 21% for B-CQDs and 19% for G-CQDs are higher than the typical values of 8–15% reported for PSI-derived CQDs under similar plasma powers and treatment durations. Moreover, the emission tunability achieved here—from 450 nm (blue) to 515 nm (green)—is realized solely by adjusting the plasma exposure time, whereas earlier studies often required dopants, additives, or post-synthetic modifications to produce comparable color shifts. The enhanced photoluminescence intensity and stability can be attributed to the controlled formation of sp^2 carbon domains and

effective surface passivation during plasma treatment. These results highlight the performance advantages and simplicity of our PSI approach compared to earlier reports.

It is also important to note that extending the plasma exposure beyond 30 minutes (e.g., 45–60 minutes) would likely lead to excessive surface oxidation and partial degradation of the carbon framework. During prolonged plasma–solution interaction, reactive species such as $O\bullet$, OH•, and NOx progressively attack the CQD surface, converting sp^2 domains into oxygen-rich amorphous carbon. This over-oxidation introduces nonradiative recombination centers, resulting in reduced photoluminescence intensity and possibly a further redshift or broadening of the emission band. These trends are consistent with previous PSI reports [10–12], where extended plasma treatment diminished luminescence efficiency due to the destruction of emissive sp^2 sites. Therefore, maintaining moderate plasma exposure durations (15–30 minutes) is crucial for achieving a balance between core carbonization and surface passivation, ensuring high quantum yield and stable emission.

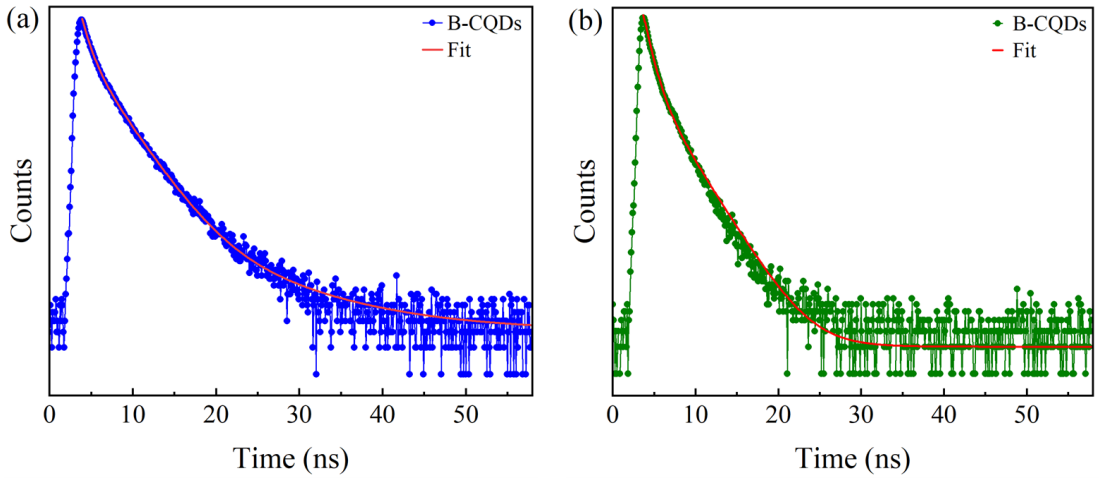

Fig. 4. (Color online) TRPL curves (λ_{ex} = 405 nm) of (a) B-CDs, (b) G-CDs.

Time-resolved photoluminescence (TRPL) measurements were performed to investigate the fluorescence decay dynamics of the synthesized B-CQDs and G-CQDs. The TRPL decay curves for both B-CQDs (Fig. 4a) and G-CQDs (Fig. 4b) were recorded under excitation at 405 nm, respectively. Both samples exhibited biexponential decay profiles, consistent with the presence of multiple radiative recombination pathways. The TRPL decay curve of B-CQDs (Fig. 4a) showed an initial fast decay component with a lifetime of τ_1 = 0.87 ns and a slower decay component with a lifetime of τ_2 = 2.89 ns. The overall fluorescence lifetime (τ_{avg}) was calculated to be 1.69 ns, indicating a rapid decay dominated by the fast recombination from the carbon core states. This result suggests that the B-CQDs exhibit strong photoluminescence originating from core π–π^* transitions within the graphitic domains of the carbon core, with a minor contribution from surface states.

For G-CQDs (Fig. 4b), the TRPL curve displayed a similar biexponential decay, but with slightly longer lifetimes: τ_1 = 0.92 ns and τ_2 = 3.25 ns, leading to an overall lifetime (τ_{avg}) of 2.49 ns. The longer decay time in G-CQDs can be attributed to the increased surface oxidation, which

introduces defect states and traps that slow down the recombination process. These defects, likely associated with oxygen-containing functional groups, contribute to the green emission through n–π^* transitions, further corroborating the interpretation of the emission mechanism observed in the steady-state PL spectra. The biexponential decay of both B-CQDs and G-CQDs is consistent with a dual-emission mechanism involving both core and surface states. The faster component (τ_1) is primarily associated with radiative recombination from the carbon core states (π–π^* transitions), while the slower component (τ_2) represents surface-related recombination processes, which are more prominent in the G-CQDs due to greater surface oxidation and the formation of defect states. The longer average lifetime of G-CQDs (τ_{avg} = 2.49 ns) suggests a more complex photophysical process compared to B-CQDs, where core emission dominates with a faster decay rate. The lifetime values obtained from TRPL analysis further support the findings from PL spectra, where B-CQDs showed blue emission dominated by the carbon core's intrinsic π–π^* transitions, and G-CQDs exhibited green emission arising from surface-state or defect-induced n–π^* transitions.

The luminescence behavior of B-CQDs and G-CQDs arises from the combined contributions of core-state and surface-state emission mechanisms. B-CQDs exhibit blue emission centered at 475 nm, primarily from π–π^* transitions within the conjugated sp^2 carbon core. This emission is fast, with an average lifetime of 0.88 ns, reflecting radiative recombination within the graphitic core. In contrast, G-CQDs show green emission at 515 nm, primarily due to n–π^* transitions associated with oxygen-containing surface functional groups and defects. The surface oxidation introduced by extended plasma exposure results in slower recombination and a longer lifetime of 3.26 ns for G-CQDs. The different emission behaviors are due to the degree of surface oxidation controlled by plasma exposure time, which influences the formation of surface defect states in G-CQDs. This dual-emission pathway, from both core and surface states, underscores the tunable photoluminescence of carbon dots, making them ideal for color-selective applications in bioimaging and optoelectronics.

3.4. In vitro bioimaging

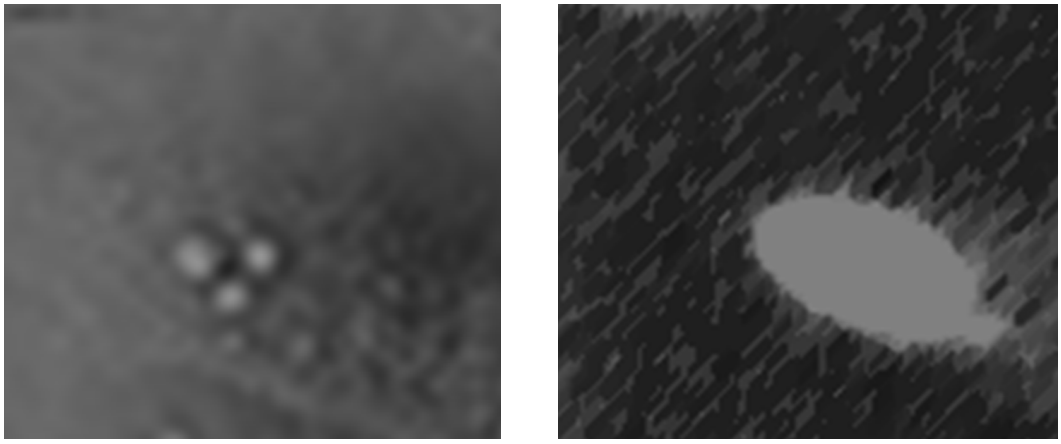

Fig. 5. (Color online) Live cell imaging of B-CQDs in Hela cells.

To evaluate the potential of the synthesized B-CQDs as fluorescent nanoprobes for biological applications, their cellular uptake and imaging capabilities were investigated in live HeLa cells. The cells were incubated with a solution of B-CQDs before being imaged with a fluorescence microscope. Fig. 5 presents the results of the live-cell imaging experiment. The bright-field images confirm that the HeLa cells maintained their typical adherent and healthy morphology after incubation, which suggests that the B-CQDs have good biocompatibility and low cytotoxicity at the tested concentration. As observed in the corresponding fluorescence channel, the cells treated with B-CQDs exhibited strong intracellular blue fluorescence. This result clearly demonstrates that the B-CQDs can effectively penetrate the cell membrane of live HeLa cells. The fluorescence signal appears to be predominantly distributed throughout the cytoplasm. Notably, distinct, brighter spots are visible within the nuclei, corresponding to the preferential accumulation of B-CQDs in the nucleoli, a common localization pattern for carbon-based nanoprobes. These findings highlight the excellent cell permeability and high-contrast imaging performance of the B-CQDs, indicating their great promise as an effective fluorescent probe for *in vitro* cellular imaging, particularly for visualizing the cytoplasm and nucleoli.

4. Conclusion

We have successfully synthesized highly photoluminescent B-CQDs and G-CQDs through a simple and environmentally friendly plasma solution interaction method using glucose as a sustainable carbon source. The plasma-assisted process enables direct control over emission wavelength by tuning the plasma exposure time, offering a clean, catalyst-free route for color-selective nanomaterial fabrication. Structural and spectroscopic analyses confirmed that both types of CQDs possess quasi-spherical morphology, nanoscale dimensions (3–5 nm), and partially graphitic cores with rich oxygen-containing surface groups. The B-CQDs exhibited blue emission at 450 nm with a quantum yield of 21%, primarily arising from core-related π–π^* transitions, while the G-CQDs showed green emission at 515 nm with a quantum yield of 19%, attributed to surface-state n–π^* transitions. Both samples demonstrated excellent photostability, dispersibility, and biocompatibility, producing strong intracellular fluorescence in *in vitro* bioimaging tests. This study highlights the plasma solution interaction method as an efficient and controllable synthesis route for producing color-tunable, biocompatible carbon dots without chemical dopants or harsh reaction conditions. The approach provides valuable insight into plasma-driven carbonization and surface passivation mechanisms, paving the way for scalable production of next-generation fluorescent probes for optical and biomedical applications.

Acknowledgements

This work is supported by Project No. CSCL05.03/25-26 of Vietnam Academy of Science and Technology (VAST). The authors are grateful for the use of the facilities of Joint Optics and Photonics Laboratory at Institute of Physics, VAST.

Authors contribution

P.V. Duong, N. M. Hoa, D. M. Hieu, Vu Van Thu conceived the experiment. Le Duc Toan, Nguyen Dac Dien and L. A. Thi conducted the experiments and analyzed the data. All authors participated in the discussion of the results; P. V. Duong, N. T. Binh, S. A. Tikhomiorv and L.

A. Thi wrote the initial draft of the paper. N. T. Binh, L. A. Thi and P. V. Duong supervised the project. All authors have read and agreed to the published version of the manuscript.

Conflict of interest

The authors declare that they have no known competing financial interests or personal relationships that could have appeared to influence the work reported in this paper.

References

[1] X. Yao, R. E. Lewis and C. L. Haynes, *Synthesis processes, photoluminescence mechanism, and the toxicity of amorphous or polymeric carbon dots*, Acc. Chem. Res. **55** (2022) 3312.
[2] Q. Xu, H. Cai, W. Li, M. Wu, Y. Wu and X. Gong, *Carbon dot/inorganic nanomaterial composites*, J. Mater. Chem. A **10** (2022) 14709.
[3] Y. Li, Q. Li, S. Meng, Y. Qin, D. Cheng, H. Gu *et al.*, *Ultrabroad-band, white light emission from carbon dot-based materials with hybrid fluorescence/phosphorescence for single component white light-emitting diodes*, Chin. Chem. Lett. **34** (2023) 107794.
[4] L. Ai, Z. Song, M. Nie, J. Yu, F. Liu, H. Song *et al.*, *Solid-state fluorescence from carbon dots widely tunable from blue to deep red through surface ligand modulation*, Angew. Chem. **135** (2023) e202217822.
[5] J. Lin, L. Wang, Q. Jing and H. Zhao, *Highly efficient and high color rendering index multilayer luminescent solar concentrators based on colloidal carbon quantum dots*, Chem. Eng. J. **481** (2024) 148441.
[6] Y. Wang, Y. Qin, W. Tian, H. Zhang, F. Wang, X. Yan *et al.*, *Dye-incorporated carbonized polymer dots with tunable solid-state emission based on intraparticle förster resonance energy transfer*, Adv. Funct. Mater. **34** (2024) 2402825.
[7] X. Xu, R. Ray, Y. Gu, H. J. Ploehn, L. Gearheart, K. Raker *et al.*, *Electrophoretic analysis and purification of fluorescent single-walled carbon nanotube fragments*, J. Am. Chem. Soc. **126** (2004) 12736.
[8] V. D. Pham, A. T. Le, M. H. Do, T. H. Le Thi, D. T. Nguyen, H. M. Pham *et al.*, *Surface modification of nitrogen-doped carbon quantum dots for enhanced functionalities*, Comm. Phys. **34** (2024) 413.
[9] K. Jiang, S. Sun, L. Zhang, Y. Lu, A. Wu, C. Cai *et al.*, *Red, green, and blue luminescence by carbon dots: Full-color emission tuning and multicolor cellular imaging*, Angew. Chem. Int. Ed. **54** (2015) 5360.
[10] N. Thanh Binh, P. Van Duong, D. Hoang Tung, P. Hong Minh and D. Thi Kieu Anh, *The effect of fabrication conditions on optical characteristics of cqds prepared by micro plasma*, Vietnam J. Sci. Technol. **63** (2025) 1107.
[11] D. H. Tung, T. T. Thuong, N. D. Cong, N. T. Liem, N. Van Kha, L. H. Manh *et al.*, *Facile synthesis of carbon quantum dots by plasma-liquid interaction method*, Comm. Phys. **27** (2017) 311.
[12] M. H. Nguyen, D. T. Le, H. T. Do and A. T. Le, *Remarkable luminescent carbon quantum dots: green synthesis from orange juice using microplasma-liquid method*, Fullerenes Nanotub. Carbon Nanostruct. **32** (2024) 282.
[13] P. Van Duong, L. Anh Thi, L. Duc Toan, P. Hong Minh, N. Thanh Binh, D. Hoang Tung *et al.*, *Size-dependent optical properties and exciton self-trapping emission in carbon quantum dots*, ChemistrySelect **9** (2024) e202401754.
[14] H. Singh, A. Bamrah, M. Khatri and N. Bhardwaj, *One-pot hydrothermal synthesis and characterization of carbon quantum dots (cqds)*, Mater. Today Proc. **28** (2020) 1891.
[15] J. B. Essner, C. H. Laber and G. A. Baker, *Carbon dot reduced bimetallic nanoparticles: Size and surface plasmon resonance tunability for enhanced catalytic applications*, J. Mater. Chem. A **3** (2015) 16354.